Published in final edited form as:
Acta Biomater. 2015 March ; 14: 1–10. doi:10.1016/j.actbio.2014.11.045.

Silk-tropoelastin protein films for nerve guidance

James D. White[a], **Siran Wang**[a], **Anthony S. Weiss**[b,c,d], and **David L. Kaplan**[a,*]

[a]Department of Biomedical Engineering, Tufts University, 4 Colby St. Medford, 02155 MA, USA

[b]School of Molecular Bioscience, University of Sydney, NSW, 2006, Australia

[c]Bosch Institute, University of Sydney, NSW, 2006, Australia

[d]Charles Perkins Center, University of Sydney, NSW, 2006, Australia

Abstract

Peripheral nerve regeneration may be enhanced through the use of biodegradable thin film biomaterials as highly tuned inner nerve conduit liners. Dorsal root ganglion neuron and Schwann cell responses were studied on protein films comprised of silk fibroin blended with recombinant human tropoelastin protein. Tropoelastin significantly improved neurite extension and enhanced Schwann cell process length and cell area, while the silk provided a robust biomaterial template. Silk-tropoelastin blends afforded a 2.4 fold increase in neurite extension, when compared to silk films coated with poly-d-lysine. When patterned by drying on grooved polydimethylsiloxane (3.5 μm groove width, 0.5 μm groove depth), these protein blends induced both neurite and Schwann cell process alignment. Neurons were functional as assessed using patch-clamping, and displayed action potentials similar to those cultured on poly(lysine)-coated glass. Taken together, silk-tropoelastin films offer useful biomaterial interfacial platforms for nerve cell control which can be considered for neurite guidance, disease models for neuropathies, and surgical peripheral nerve repairs.

Keywords

nerve regeneration; nerve guide; silk; elastin; protein blends

1. Introduction

Peripheral nerve injuries occur in ~3% of trauma patients, and greatly affect quality of life for recovering patients (1, 2). Functional recovery is dependent upon the severity of injury (gap size), denervation time, and age of the patient. About 50% of surgical repairs promote

*Corresponding author. david.kaplan@tufts.edu (D.L. Kaplan), Tel: 617-627-3251, Fax: 617-627-3231.

Conflict of interest
None

normal restoration of function (3, 4) and quality of life effects range from life-long disabilities to complaints of clumsiness, sensitivity, pain, and inability to work (5, 6). An outstanding clinical need is the development of nerve conduits that support the regeneration of long gap nerve repairs (> 3 cm), for which no FDA-approved biomaterial is currently available. Autologous grafting is considered the gold standard for peripheral nerve repair. The development of new biomaterials will present an attractive alternative to autologous nerve grafting procedures, by not requiring follow-up surgery that risks donor site morbidity and donor nerve mismatch (7). Currently, direct suturing of the nerve fiber, autologous grafting, and the use of biocompatible nerve guides are available treatment options for nerve transection injuries (8). Several studies using nerve conduits composed of natural (9–11) or synthetic materials (12–16) have shown potential for nerve conduits. Current commercial (<3 cm) nerve guides include Neurolac (poly(DL-lactide-ε-caprolactone)(17), NeuroTube (poly(glycolic acid)(18), and NeuraGen (type 1 collagen)(19). These nerve conduits present surgeons with materials that facilitate peripheral nerve repair and display low immunogenicity.

Protein formulations using biocompatible polymers can be cast into thin films and used as inner guide liners to nerve guides (20). When fabricated in this way, they may interact directly with regenerating nerve fibers to promote optimal growth, while only necessitating small amounts of the biomaterial. Protein blending provides a way to improve cell responses to scaffolds, by allowing systematic tuning of the surface structure, chemistry, charge and topography. Often, nerve guides are fabricated from a single biomaterial. Here, we hypothesize that blending silk protein with recombinant human tropoelastin will improve the performance of silk fibroin protein conduits currently being developed.

In our previous studies of silk-tropoelastin protein films, we found that the surface charge and roughness may be systematically tuned by simple protein blending(21). We have also shown the benefit of this approach in the response of central nervous system cortical neurons on silk-tropoelastin blends, where the charge density was critical to cellular response (22). Mechanistically, the complementary charges of silk and tropoelastin provide a platform for systematic alteration of surface charge and elastic modulus. Silk fibroin is a large protein (~400 kDa), with an overall negative charge, and has shown considerable promise as an FDA approved biomaterial for nerve repair (23). Tropoelastin is the monomer protein unit of elastin, can improve cell growth, and is a smaller protein (60 kDa) with an overall positive charge (24). Tropoelastin displays biocompatibility, and improves cell adhesion including fibroblasts (25), chondrocytes (26), smooth muscle cells (27), and endothelial cells (28).

Our goal was to study peripheral neuron and Schwann cell growth on silk-tropoelastin films for peripheral nerve regeneration, including growth responses and functional generation of action potentials, a key requirement for conveying sensory information between the peripheral and central nervous systems (29). We found that increases in tropoelastin content enhanced neuron density and neurite growth. Schwann cell spreading and process length was also increased when cultured on the blend films. Films were fabricated with patterns to promote neuron alignment, and found to support the generation of action potentials with a similar efficacy to the positive control (poly(lysine)-coated glass (PDL-glass).

2. Materials and Methods

2.1 Preparation of silk-tropelastin films

Silk fibroin solution was prepared using our previously published methods (30). Briefly, silk cocoons (*Bombyx mori*) were boiled in a Na_2CO_3 solution (0.02 M) to remove sericin proteins, dissolved using LiBr solution (9.3 M), and dialyzed using distilled water to afford an aqueous silk solution (~6–8% wt/vol). Tropoelastin was purified using a bacterial multigram expression system for SHELΔ26A (synthetic human elastin without domain 26A) corresponding to amino acid residues 27–724 of GenBank entry AAC98394 (gi182020) (31, 32). Protein blends were prepared by mixing the aqueous silk solution (5% wt/vol) with an aqueous tropoelastin solution (5% wt/vol) at 0°C. Films were prepared containing 0%, 10%, 25%, 50%, and 75% wt/wt of tropoelastin, and are designated as SE0, SE90, SE75, SE50, and SE25 respectively. The protein solutions (50 μL) were spread onto glass coverslips (15 mm diameter) and allowed to dry at room temperature overnight. Patterned silk-tropoelastin films were prepared by drying the protein mixtures on patterned polydimethylsiloxane (PDMS) molds with a grooved surface with groove widths of 3.5 μm and depths of 0.5 μm. β-sheet cross-linking for the silk protein was induced by water-annealing as we have previously reported (33). The blend films were placed in a vacuum oven, and boiling water (400 mL) was added to an inserted tray. Vacuum was applied (~25 mm Hg), and the samples were incubated (relative humidity above 90%) for 2 h at pressure. The samples were sterilized using ultraviolet radiation prior to cell seeding. For neuron viability, neurite extension analysis, Schwann cell growth and cell alignment cells were seeded onto 2–3 independent films for each condition. Comparison to poly(lysine)-coated silk fibroin films were made for each experiment, as poly(lysine) treatment is a commonly used to increase neuron attachment. Poly(lysine) at 10 and 100 μg/mL was adsorbed to the silk fibroin films for 2 h, and the films were washed (2×) with PBS.

2.2 Isolation and dissociation of embryonic chick dorsal root ganglion neurons

Fertilized eggs were obtained from the University of Connecticut Poultry Farm. Dorsal root ganglion (DRG) explants were isolated and dissociated to obtain cell suspensions for seeding peripheral neural cell culture experiments. The explants were isolated from E8–9 chick embryos as previously reported (34) and in accordance with Tufts ICAUC regulations. Briefly, chick embryos were removed from eggs, decapitated using surgical scissors, and immobilized on a poly(dimethylsiloxane) (PDMS) microsurgery stage. Once the ventral organs were removed, DRGs were gently removed using surgical forceps from either side of the vertebral column in the thoracic region and stored in Hank's Buffered Saline Solution supplemented with dextrose (6 mg/mL) and sodium bicarbonate (0.35 mg/mL). For dissociation, explants were trypsinized for 25 min at 37°C, centrifuged, resuspended, and triturated several times to obtain a homogenous cell suspension. Reverse panning (45 min on tissue culture plastic) was conducted to remove large residual tissue pieces and fibroblasts (which adhere faster than neurons) to improve neuron purity. The dissociated neurons were grown in DMEM/F12 medium supplemented with FBS (10%) and nerve growth factor (NGF) (50 ng/mL, R&D Systems, Minneapolis, MN). Neurons (75,000 or 25,000 cells) were seeded onto the films in a volume of 40 μL. The neurons were allowed to adhere to the

surface for ~30 min, and then 1 mL of cell culture media was added to each well in a 24-well plate.

2.3 Schwann cell culture

Schwann cells were obtained from ATCC (*Rattus norvegicus*, CRL-2768) and cultured using DMEM supplemented with FBS (10%) and penicillin/streptomycin. Schwann cells (~10,000 cells) were seeded onto silk-tropoelastin films using a volume of 40 μL, allowed to adhere for ~30 min, and 1 mL of cell culture media was added to each well in a 24-well plate.

2.4 Viability and Cell Proliferation Assays

Dissociated chick embryonic neurons (E8–9) were grown on silk films for a period of two weeks, with Alamar blue quantification recorded on days 1, 3, 5, and 14, as the average value for three films. Medium was removed from each sample, and the sample incubated with media supplemented with Alamar blue reagent (10% vol/vol) for 2 h at 37 °C. Following incubation, the fluorescence was recorded using an excitation wavelength of 530 nm, and an emission wavelength of 590 nm.

Ki-67 and DAPI nuclear staining were conducted for DRG neurons grown on the protein blends to determine cell attachment and the percentage of proliferative cells present (Ki-67 positive). Cultured neurons were fixed using paraformalehyde (4% solution in PBS) and washed 3× using PBS. The cells were blocked and permeabilized using a triton solution (0.01% w/v in PBS) containing 10% goat serum. Ki-67 (Abcam, anti-rabbit, 1:500 dilution) was applied and the cells were stained at 4 °C overnight. The cells were washed 3× with PBS and incubated with secondary antibody IgG-FITC (Sigma, anti-rabbit, 1:100 dilution in PBS supplements with 2% FBS) for 30 min. The cells were washed with PBS containing DAPI (1:10,000 dilution), washed several times with PBS, and imaged using Leica fluorescence microscope (Leica DM IL, Buffalo Grove, IL) using FITC and DAPI filters. The percentage of prolifertive cells was calculated as the number of Ki-67 stained nuclei divided by the number of DAPI-stained nuclei.

2.5 Immunostaining dorsal root ganglion neurons with Anti-Tubulin β-III

Cultured neurons were fixed using paraformaldehyde (4% solution in PBS) for thirty minutes at room temperature. The paraformaldehyde was removed, and the cells were washed 3× (5 min each wash) with PBS. The cells were permeabilized using Triton X-100 (0.3% v/v in PBS) for 5 min, washed (2× 5 minutes), and treated with anti-tubulin β-III (Sigma, anti-rabbit, 1:500 dilution in PBS supplemented with 10% FBS) overnight at 4 °C. The cells were washed (3× 5 min), incubated with secondary antibody IgG-FITC (Sigma, anti-rabbit, 1:100 dilution in PBS supplements with 2% FBS) for 30 min. The cells were washed (3× 5 min), and imaged in PBS solution. Fluorescent images were collected using a Leica fluorescence microscope (Leica DM IL, Buffalo Grove, IL) using a FITC filter. Image analysis was conducted using ImageJ software (National Institute of Health, Bethesda, MD) (35).

2.6 Fluorescent staining of Schwann cells with Phalloidin

Schwann cells were fixed with paraformaldehyde (4% solution in PBS) for thirty minutes, washed (3× 5 min) with PBS. The cells were permeabilized with Triton X-100 (0.3%, 5 min) and washed (2× 5 min) with PBS). To the permeabilized cells was added Alexa Fluor 488 Phalloidin (Life Technologies, Grand Island NY, 1:40 dilution in PBS containing 1% BSA) and the cells were incubated at room temperature for 2 hr. The cells were washed (3× 5 min) with PBS. Nuclear staining using 4',6-Diamidino-2-Phenylindole (DAPI, Life Technologies, Grand Island NY, 1 : 10,000 dilution in PBS) was conducted, and the cells were washed (2× 5 min) with PBS. The cells were incubated for 30 min at room temperature, and were imaged with a fluorescence microscope with FITC and DAPI filter. Cell area and process length measurements were collected using ImageJ.

2.7 Electrophysiology

Whole cell patch clamping experiments were obtained according to previously published procedures (36), using an AXOPATCH 1D Patch Clamp amplifier (Axon Instruments, Sunnyvale, CA) and Axon CNS Molecular Devices Digidata 1440A Low-Noise Data Acquisition System (Axon Instruments, Sunnyvale, CA). Electrophysiological recording was performed on days 3–5 *in vitro*. Thin-walled borosilicate glass capillaries were pulled into patch pipettes using a Flamin/Brown Micropipette Puller, Model P-87 (Sutter Instrument, Novato, CA). Membrane potentials were determined using voltage-clamp mode, while current-clamp was used for current injection experiments to induce action potentials. Extracellular solution composition was NaCl (140 mM), KCl (2.8 mM), $CaCl_2$ (2 mM), $MgCl_2$ (2 mM), HEPES (10 mM), Glucose (10 mM). Intracellular solution composition was Potassium Gluconate (140 mM), NaCl (10 mM), $MgCl_2$ (2 mM), HEPES (10 mM), EGTA (1 mM), Mg-ATP (4 mM), and Na-GTP (0.3 mM). Experiments were conducted at room temperature.

2.8 Statistical analysis

All data analysis was performed with one way analysis of variance (ANOVA) followed by Dunnett's post hoc test to determine statistical significance. Statistical significance is designated with *$p<0.05$, **$p<0.01$, and ***$p<0.001$. Neurite extension, Schwann cell length, and Schwann cell area are presented as the average value, with the standard error of the mean reported. Cell attachment at various time points and percent proliferative cells were determined from three random fields of view for each blend. Quantification of neurite extension, schwann cell process length, and Schwann cell area were calculated from a total of 6 random fields of view for each blend (two fields of view randomly selected from three separate films (N=6) using a single culture.

3. Results and Discussion

3.1: Protein blending

Aqueous silk and tropoelastin protein solutions were prepared at 5% (w/v) and cooled on ice. The proteins were mixed with varying ratios and cast onto glass microscope slides. Drying at room temperature and water annealing afforded insoluble films to compare dorsal

root ganglion and Schwann cell response. The dried protein films contained ~1.4 mg of total protein per square centimeter. With these processing parameters, the films were strong enough to be physically detached from PDMS substrates, which was necessary for patterning experiments or nerve guide fabrication.

The blended films from silk and tropoelastin have tunable surface charges ranging from anionic (−36 total charge) to cationic (+36 total charge). As tropoelastin content is increased, the elastic modulus decreased (37). For water annealed silk-tropoelastin blends, a Young's modulus of ~25 and 5 MPa was reported for silk films alone, and blended with 50% tropoelastin content, respectively (37). Rat sciatic nerve, a common model for *in vivo* peripheral nerve repair studies, displays an elastic modulus of ~0.58 MPa (38). The silk-tropoelastin films are significantly stiffer, with films containing greater tropoelastin within an order of magnitude the stiffness of native tissue. While strong, we find the silk alone films are able to be sutured using 9-0 nylon sutures when hydrated. Taken together, these properties afford an adaptable protein system for optimizing cell growth.

3.2 Embryonic dorsal root ganglion neuron cell growth and viability

Dissociated embryonic chick dorsal root ganglion neurons were grown on silk-tropoelastin protein surfaces. Dissociated chick DRG neurons were chosen as a model system for our study as it provides a primary neuron cell type, allows rapid isolation of neurons for multiple experiments, and has been previously utilized for both 2D and 3D studies of neuronal growth (39–42).

Increased tropoelastin content (SE50 and SE25 films) yielded higher metabolic activity compared to silk alone, poly(lysine-coated silk), and SE90 silk films over two weeks (Figure 1). After two weeks, compared to silk alone, the SE50 and SE25 showed a 8.15 and 8.02 fold increase in metabolic activity. The high metabolic activity was considered to relate to the combined effects of increased Schwann and fibroblast proliferation with neuron metabolic activity. Cell attachment was quantified at days 1, 3, and 5 using DAPI staining. A trend towards increase in cell attachment for blends with higher tropoelastin contents (SE 75, 50, and 25) was observed, The fraction of proliferative cells was similar for each blend condition (~ 0.1 – 0.35%) suggesting that both cell attachment and modulation of cell activity may both contribute towards the Alamar metabolic activity readout. Following two weeks in culture, adherent neuronal clusters were observed (βIII tubulin immunostaining) for silk-tropoelastin blends with 50 and 75% tropoelastin, respectively, while films with lower tropoelastin content failed to show attached neurons.

3.3 Neurite Outgrowth Analysis

To examine the effect of tropoelastin-addition on neuron regeneration, neurite outgrowth was quantified using Anti-Tubulin III staining for dissociated DRG cultures after four days of growth. Tubulin staining was chosen as it provides bright and reliable staining of embryonic chick DRG neurons. DRG neurites extend rapidly, and can reach up to ~300 μm per day (43). A four-day culture time was chosen to allow long neurite extension (up to ~1000 μm) allowing the structure-function relationship of blend ratio to neurite extension to be discerned. Previous studies with dissociated embryonic chick dorsal root ganglion

neurons typically quantify neurite outgrowth in the 1–4 day time regime (39–42). Representative images of neuron density and neurite outgrowth on each protein blend are shown in Figure 2A. In addition to the silk films alone, dissociated DRG neurons were also grown on films that were coated with poly-D-lysine (PDL). PDL is commonly used to promote neuron attachment to surfaces. Two concentrations of PDL (designated herein as L PDL and H PDL for 10 μg/mL and 100 μg/mL coating solutions respectively) were used to promote neuron attachment (44, 45). The PDL-coated silk films also provided a control to observe the effects of neuron growth by introducing a positively charged coating, without changes in elastic modulus of the films. Neurite growth was studied using two cell seeding densities (43,000 and 13,000 cells/cm^2).

When seeded at the higher concentration, the density of neurons was highest for the silk-tropoelastin blends that contained higher percentages of tropoelastin (50 and 75% w/w tropoelastin). DAPI nuclear staining shows increased cell number for protein blends with 50 and 75% tropoelastin content (Figure 2A). Quantification of neurite outgrowth was measured using the NeuronJ plugin with Image J (Figure 2B). Neurite extension on silk alone, SE90, and the PDL-coated silks were statistically the same, with an average value of 326 ± 47 μm. Silk-tropoelastin blends with greater than 25% tropoelastin content (SE25, SE50, and SE75) each produced statistically significantly longer neurite extensions after 4 days in culture than the silk alone, 10% SE90, and PDL-coated silk samples, with average neurite lengths ranging from 476 to 627 μm. The longest average neurite extension was observed on the silk-tropoelastin (25/75%) blend. This may be due to the protein surface promoting strong neurite outgrowth, but on a surface that generates lower neuron attachment and therefore larger average interneuron distance. With a tropoelastin content less than or equal to 10%, sparser numbers of neurons with few attachments were observed. Table 1 summarizes average values for the median neurite measured per image, the longest neurite measured per image, and the neuron cluster density for each condition. Consistent with the mean neurite lengths, the median and longest neurites recorded for the higher tropoelastin blends (25, 50, and 75% w/w) were larger than on the silk and silk-PDL surfaces. Quantification of neuron cluster density showed a systematic increase in neuron attachment as the tropoelastin content was increased in the films from 10% to 75% (w/w). Similarly, coating with 10 μg/mL and 100 μg/mL PDL led to increased neurons density of 1.4 ± 0.9 and 2.1 ± 1.1 neuron clusters/mm^2 from the 0.9 ± 0.04 clusters/mm^2 for silk alone. The silk-tropoelastin blends outperformed the silk-PDL coatings, producing ~4.3 and 4.4 clusters/mm^2 for silk-tropoelastin with 50 and 75% (w/w) content, respectively.

As neuron number and cell-cell contact may affect neuron growth, we also measured neurite extension on the blend films using a lower cell seeding density. In this way, more isolated neuron growth was quantified. Measurement of these neurite extensions show that the SE75 films produced significantly longer neurite extensions compared to the SE100, SE100 LPDL, and SE100 H PDL control groups (Figure 2B).

Recently, synthetic scaffolds incorporating positively charged functional groups have been investigated for effects on neuron adhesion and neurite extension. The improved response of DRG extension is consistent with these findings which showed that systematic addition of cationic charge to oligo-(polyethylene glycol) fumarate-based hydrogels led to increased

neurite extension until an optimal charge concentration was reached (46). As the content increased there was a subsequent decrease in neurite extension; at very high charge density. Increases in neuron adhesion and viability until a critical positive charge concentration was also reported for mice hippocampal cells on PEG-based hydrogels modified with positively-charged acetycholine functional groups (47). The decrease in neurite extension in synthetic hydrogel systems at high charge content may be attributed to increased concentrations of trimethylammonium chloride groups, which may be less biocompatible than the protein-based materials in silk-tropoelastin films. The addition of natural proteins may offer biomaterials with improved cell viability. For example, collagen addition to poly(L-lactide-co-glycolic acid) neural tubes has shown efficacy for neuron regeneration (48). Similar to the present work, we recently examined silk-tropoelastin films for cortical neuron growth (22). Cortical neuron attachment and viability was optimal with intermediate tropoelastin content (22). Interestingly, for peripheral neurons, a slightly different result was found, with strong neuronal growth maintained even at higher tropoelastin contents. These results may be attributed to differences in cortical neuron biology, compared to peripheral neurons. Different neurite outgrowth between peripheral and central nervous system neurons has been documented for substrates coated with fibronectin or laminin proteins (49). Peripheral neurons are enhanced by each of these extracellular proteins, while spinal cord and retinal neurons (central nervous system) show improved outgrowth with laminin, but aggregate and fail to produce extensions on fibronectin coated plastic. Our previous results with cortical neurons grown on silk-tropoelastin films show neurite extension effects similar to fibronectin coatings (22).

In addition to surface charge considerations, neuron attachment and neurite extension are also dependent upon the film or gel mechanical properties. Balgude et al. report an increase in neurite extension with decreasing gel stiffness for agarose gels with storage modulus from ~ 20–1300 dyne/cm^2) (42). Similarly, Zuidema found that polysaccharide gels showed greater neuron attachement and growth as the gels became softer and more positively charged (50). These results generally suggest lowering the stiffness of the material increases neurite extension. In contrast however, a controlled study of neuron growth on PDL-coated PDMS surfaces ranging from 18 to 1882 kPa, higher cell attachment and neurite growth was found on one of the slightly stiffer surfaces (~88 kPa) (51). Our present study demonstrates that increases in neurite extension for DRG neurites may also be obtained by simply tuning the blending ratio of silk fibroin and tropelastin proteins.

3.4 Schwann cell growth analysis

To complement increased neurite outgrowth on silk-tropoelastin blends, the growth of Schwann cells on the silk-tropoelastin films was studied. Schwann cells play a significant role in nerve regeneration through several mechanisms including production of neurotrophic factors (52, 53) and myelination of the regenerating axons (54). Furthermore, increased Schwann cell migration/presence at regenerating site has been shown to increase the efficacy of peripheral nerve repair in *in vivo* studies (23). We hypothesize that surfaces favorable to Schwann cell attachment and elongation may provide improved functional outcomes of PNR. Rat Schwann cells were cultured on tropoelastin-silk films, and grew rapidly on each of the surfaces. The Schwann cell area and cell process length was

quantified using f-actin staining (phalloidin). Protein blends with tropoelastin afforded statistically higher cell spreading areas compared to Silk H PDL, and consistently trended towards higher values than Silk L PDL and SE100 films. With a small addition of tropoelastin, the SE90 films afforded cell area and process lengths that were statistically larger than the SE100 films alone.

The promotion effect of tropoelastin towards increased cell attachment and cell spreading was similar to the work of Gu (55) and our previous results obtained for human mesenchymal stem cells (hMSCs) grown on the silk-tropoelastin blends (21). Gu et al. recently provided the first study on the effect of substrate stiffness on Schwann cell biology (55). When grown on polyacrylamide surfaces ranging from 4–12 kPa stiffness, Schwann cells on the 7 kPa condition showed a significant increase in viability, surface area of adherent cells, cell elongation, and release of neurotrophic factors. Silk-tropoelastin blends promoted a more elongated hMSC morphology, while hMSCs grown on silk alone displayed spherical morphology, with an expected lower viability (21). Bipolar elongation of processes is an important cytoskeletal structural feature, and allows Schwann cells to form the mylenin internode. Adopting this more differentiated morphology may be indicative of improved Schwann cell function during nerve repair (Thaxton). Schwann cell process length also trended towards higher values for silk-tropoelastin blends than the control conditions. The SE90, SE75, SE50 and SE25 average process length were statistically higher than PDL-coated silk (100 μg/mL). The SE90 films were statistically higher than the S100 films.

3.5 Patterned neurite and Schwann cell growth

Achieving alignment of neurite extensions and Schwann cell processes is an important benchmark for the development of nerve guides (56). The neurons and Schwann cells displayed aligned growth by patterning the silk-tropoelastin films. Previous studies in our laboratory of aligned growth on silk films have shown that groove patterns with dimensions 3.5 μm wide and 0.5 μm deep were are able to align neurite growth using P19 and SH-SY5Y stem cell derived neurons (57). With embryonic chick dorsal root ganglion neurons, neurite alignment was achieved using the silk-tropoelastin films and Image J was used to measure the angle of deviation from the groove angle. The average angle from deviation was similar for each surface type, with average deviations of 26 ± 22°, 21 ± 20°, and 22 ± 22° for S100 (N=78), S50 (N=153) and S25 (N=135) surfaces, respectively. The angle deviations were plotted in histograms and the fraction of neurites at each 10° increment was measured (Figure 4b). The patterned films afforded neurite alignment with 33%, 43%, and 41% of neurites within 10° of the groove angle for the S100, S50, and S25 surfaces, respectively (Figure 4b). Schwann cells similarly display aligned processes using the blended materials with the 60–70% of processes showing alignment within 20° of the patterned groove direction (Figure 4b). This demonstrated that the patterned silk films and silk-tropoelastin films could guide neuron growth and therefore are candidates for nerve guidance.

3.6 Electrophysiological characterization of DRG neurons grown on silk-tropoelastin films

Patch-clamp experiments were used to investigate the electrophysiological function of the cultured neurons on silk-tropoelastin surfaces. The silk-tropoelastin blends with highest tropoelastin content (50 and 75% tropoelastin) adhered to negatively charged glass

coverslips to facilitate patch-clamping experiments. Neurons were grown on the silk-tropoelastin films as well on PDL-coated glass controls. The resting membrane potential of the neurons, as well as the current-induced neuron depolarization and action potentials were quantified (Figure 5a). On PDL-coated glass, the neurons displayed a resting potential of −43 ± 0.1 mV (n=2). Embryonic chick DRGs have reported resting membrane potentials of −50 ± 1.2 mV (34, 58). For neurons grown on the silk-tropoelastin films with 50 and 75% tropoelastin (w/w) contents, resting membrane potentials of −50 ± 5 mV and −48 ± 8 mV, respectively, and do not significantly differ from neurons cultured onto PDL-coated glass (Figure 5b). Importantly, neurons on the silk-tropoelastin films generated action potentials when depolarized. Similarly, the magnitude of the action potential approached ~100 mV for each of the three groups, and was not significantly different. The ability of each film to produce a characteristic 100 mV action potential suggested appropriate expression and function of sodium channels. The silk-tropoelastin films showed minimal baseline activity for generating action potentials, suggesting successful electrophysiological function of the neurons on the protein surfaces.

4. Conclusions

Silk-tropoelastin blends in film form supported peripheral neuron and Schwann cell growth, with increased tropoelastin content (25–75%) providing a combination of improved Schwann cell growth and neurite extension. The tropoelastin was also beneficial towards effecting increased Schwann cell spreading and process length. Schwann cells play a significant role in peripheral neuron repair, and recent efforts towards achieving increased Schwann cell recruitment and alignment show promise towards improving the efficacy of nerve repair (59). For both the Schwann cells and DRG neurites, extension alignment was achieved using a patterning strategy to introduce grooves onto the surfaces of the protein films. Neurites and Schwann cell processes grew on patterned films and showed a majority of extensions within 20° of the groove direction. Neuron electrophysiological activity showed similar action potentials for neurons grown on PDL-coated glass and the silk-tropoelastin films. Importantly, the silk-tropoelastin films are transparent and flexible, providing additional options for utility as biomaterials for neural repairs.

Supplementary Material

Refer to Web version on PubMed Central for supplementary material.

Acknowledgements

The authors thank Dr. Chuang Du for his expertise and assistance with electrophysiological experiments, and Dr. Min Tang-Schomer, Dr. Lee W. Tien, Dr. Amy Hopkins and Prof. Cristian Staii for insightful discussions. The authors also thank the NIH P41 Tissue Engineering Resource Center (P41 EB002520). ASW is Scientific Founder of Elastagen Pty Ltd. ASW acknowledges grant support from the Australian Research Council and the National Health & Medical Research Council. Part of this research was funded by NIH EB014283 (DLK and ASW).

References

1. Noble JMC, Prasad VS, Midha R. Analysis of upper and lower extremity peripheral nerve injuries in a population of patients with multiple injuries. J Trauma. 1998; 45:116–122. [PubMed: 9680023]

2. Gu XDF, Yang Y, Liu Jie. Construction of Tissue Engineered Nerve Grafts and their Application in Peripheral Nerve Regeneration. Prog Neurobiol. 2011; 93:204–230. [PubMed: 21130136]

3. Scholz T, Krichevsky A, Sumarto A, Jaffurs D, Wirth GA, Paydar K, Evans G. Peripheral nerve injuries: an international survey of current treatments and future perspectives. J Reconstr Microsurg. 2009; 25(6):339–344. [PubMed: 19301234]

4. Battiston BRS, Tos P, Gaidano V, Audisio C, Scevola A, Perroteau I, Geuna S. Tissue engineering of peripheral nerves. Int Rev Neurobiol. 2009:227–249. [PubMed: 19682640]

5. Thorsen FRH, Steen Carlsson K, Dahlin LB. Digital nerve injuries: epidemiology, results, costs, and impact on daily life. J Plast Surg Hand Surg. 2012; 42(3–4):184–190. [PubMed: 22686434]

6. Isaacs J. Major peripheral nerve injuries. Hand Clin. 2013; 3:371–382. [PubMed: 23895717]

7. Cunha C, Panseri S, Antonini S. Emerging nanotechnology approaches in tissue engineering for peripheral nerve regeneration. Nanomedicine: NBM. 2011; 7:50–59.

8. Nectow ARMK, Kaplan DL. Biomaterials for the development of peripheral nerve guidance conduits. Tissue Eng Part B Rev. 2012; 1:40–50. [PubMed: 21812591]

9. Taras JSJS, Lincoski CJ. Reconstruction of digital nerves with collagen conduits. J Hand Surg Am. 2011; 36(9):1441–1446. [PubMed: 21816545]

10. Wang HZQ, Zhao W, Liu Q, Gu X, Yang Y. Repairing rat sciatic nerve injury by a nervegrowth-factor-loaded chitosan-based nerve conduit. Biotechnol Appl Biochem. 2012; 59(5):388–394. [PubMed: 23586915]

11. Yang YDF, Wu J, Hu W, Liu W, Liu J, Gu X. Development and Evaluation of Silk Fibroin-based Nerve Grafts for Peripheral Nerve Regeneration. Biomaterials. 2007; 28:5526–5535. [PubMed: 17884161]

12. Reid, AJdLA.; Faroni, A.; Downes, S.; Sun, M.; Terenghi, G.; Kingham, PJ. Long term peripheral nerve regeneration using a novel PCL nerve conduit. Neurosci Lett. 2013; 544:125–130. [PubMed: 23583695]

13. Suwantong OWS, Sanchavanakit P, Pavasant P, Cheepsunthorn T, Bunaprasert T, Supaphol P. In vitro biocompatibility of electrospun poly(3-hydroxybutyrate) and poly(3-hydroxybutyrate-co-hydroxyvalerate) fiber mats. Int J Biol Macromol. 2007; 40:217–223. [PubMed: 16949148]

14. Lu MCHY, Lin JH, Yao CH, Lou CW, Tsai CC, Chen YS. Evaluation of a multi-layer microbraided polylactic acid fiber-reinforced conduit for peripheral nerve regeneration. J Mater Sci Mater Med. 2009; 20(5):1175–1180. [PubMed: 19115095]

15. de Boer RKA, Borntraeger A, Herbert-Blouin MN, Spinner RJ, Malessy MJ, Yaszemski MJ, Windebank AJ. Rat sciatic nerve repair with a poly-lactic-co-glycolic acid scaffold and nerve growth factor releasing microspheres. Microsurgery. 2011; 31(4):293–302. [PubMed: 21400584]

16. Chiono VSS, Rechichi A, Tonda-Turo C, Vozzi G, Vozzi F, D'Acunto M, Salvadori C, Dini F, Barsotti G, Carlucci F, Burchielli S, Nicotino S, Audisto C, Perroteau I, Giusti P, Ciardelli G. Poly(ester urethane) guides for peripheral nerve regeneration. Macromol Biosci. 2011; 11(2):245–256. [PubMed: 21104881]

17. Bertleff MJMM, Nicolai JP. A prospective clinical evaluation of biodegradable neurolac nerve guides for sensory nerve repair in the hand. J Hand Surg Am. 2005; 30(3):513–518. [PubMed: 15925161]

18. Agnew SP DG. Technical use of synthetic conduits for nerve repair. Journal of Hand Surgery. 2010; 35(5):838–841. [PubMed: 20381978]

19. Archibald SJSJ, Krarup C, Madison RD. Monkey median nerve repaired by nerve graft or collagen nerve guide tube. J Neurosci. 1995; 15(5):4109–4123. [PubMed: 7751969]

20. Clements IPKY, English AW, Lu X, Chung A, Bellamkonda RV. Thin-film enhanced nerve guidance channels for peripheral nerve repair. Biomaterials. 2009; 30(23–24):3834–3846. [PubMed: 19446873]

21. Hu XWX, Rnjak J, Weiss AS, Kaplan DL. Biomaterials derived from silk-tropoelastin protein systems. Biomaterials. 2010; 31:8121–8131. [PubMed: 20674969]

22. Hu X, Tang-Schomer MD, Huang W, Xia X, Weiss AS, Kaplan DL. Charge-Tunable Autoclaved Silk-Tropoelastin Protein Alloys That Control Neuron Cell Responses. Adv Funct Mater. 2013; 23(31):3875–3884. [PubMed: 25093018]

23. Lin Y, Ramadan M, Hronik-Tupaj M, Kaplan DL, Philips BJ, Sivak W, Rubin JP, Marra KG. Spatially Controlled Delivery of Neurotrohic Factors in Silk Fibroin-based Nerve Conduits for Peripheral Nerve Repair. Ann Plast Surg. 2011; 67(2):147–155. [PubMed: 21712696]
24. Mithieux SMWS, Weiss AS. Tropoelastin - A multifaceted naturally smart material. Advanced Drug Delivery Reviews. 2013; 65:421–428. [PubMed: 22784558]
25. Bax DVRU, Bilek MM, Weis AS. Cell adhesion to tropoelastin is mediated via the C-terminal GRKRK motif and integrin alphaVbeta3. J Biol Chem. 2009; 284(42):28616–28623. [PubMed: 19617625]
26. Broekelmann TJKB, Ishibaschi H, Werneck CC, Keeley FW, Zhang L, Mecham RP. Tropoelastin interacts with cell-surface glycosaminoglycans via its COOH-terminal domain. J Biol Chem. 2005; 280(49):40939–40947. [PubMed: 16192266]
27. Akhtar KBT, Song H, Turk J, Brett TJ, Mecham RP, Adair-Kirk TL. Oxidative modifications of the C-terminal domain of tropoelastin prevent cell binding. J Biol Chem. 2011; 286(15):13574–13582. [PubMed: 21321118]
28. Bax DVLS, McKenzie DR, Bilek MM, Weiss AS. Tropoelastin switch and modulated endothelial cell binding to PTFE. BioNanoScience. 2011; 1:123–127.
29. Ho COLM. Single-cell analysis of sodium channel expression in dorsal root ganglion neurons. Mol Cell Neurosci. 2011; 46(1):159–166. [PubMed: 20816971]
30. Wray LSHX, Gallego J, Georgakoudi I, Omenetto FG, Schmidt D, Kaplan DL. Effect of Processing on Silk-based Biomaterials: Reproducibility and Biocompatibility. Journal of Biomedical Materials Research B: Applied Biomaterials. 2011; 99(1):89–101.
31. Wise SGWA. Tropoelastin. Int J Biochem Cell Biol. 2009; 41:494–497. [PubMed: 18468477]
32. Martin SLVB, Weiss AS. Total synthesis and expression in Escherichia coli of a gene encoding human tropoelastin. Gene. 1995; 154:159–166. [PubMed: 7890158]
33. Jin H-JPJ, Karageorgiou V, Kim U-J, Valluzzi R, Cebe P, Kaplan DL. Water-Stable Silk Films with Reduced β-Sheet Content. Adv Funct Mater. 2005; 15(8):1241–1247.
34. Dichter MAFG. The action potential of chick dorsal root ganglion neurones maintained in cell culture. J of Physiology. 1977; 267(2):281–298.
35. Meijering EJM, Saria JCF, Steiner P, Hirling H, Unser M. Design and validation of a tool for neurite tracing and analysis in fluorescence microscopy images. Cytometry Part A. 2004; 58(2): 167–176.
36. Hamill OPMA, Neher E, Sackmann B, Sigworth FJ. Improved patch-clamp techniques for high resolution recording from cells and cell free membrane patches. Pflugers Archiv. 1981; 391(2):85–100. [PubMed: 6270629]
37. Hu XPS-H, Gil ES, Xia X-X, Weiss AS, Kaplan DL. The influence of elasticity and surface roughnes on myogenic and osteogenic differentiation of cells on silk-elastin biomaterials. Biomaterials. 2011; 32:8979–8989. [PubMed: 21872326]
38. Borschel GHKK, Kuzon WM, Dennis RG. Mechanical Properties of Acellular Peripheral Nerve. J Surg Res. 2003; 114:133–139. [PubMed: 14559438]
39. Swindle-Reilly KEPJ, Kutosky HP, Throm A, Hammer JA, Harkins AB, Willits RK. The impact of laminin on 3D neurite extension in collagen gels. J Neural Eng. 2012; 9(4):046007. [PubMed: 22736189]
40. Willits RKSS. Effect of collagen gel stiffness on neurite extension. J Biomater Sci Polym Edn. 2004; 15(12):1521–1531.
41. Blewitt MJWR. The effect of soluble peptide sequences on neurite extension on 2D collagen substrates and within 3D collagen gels. Ann Biomed Eng. 2007; 35(12):2159–2167. [PubMed: 17934866]
42. Balgude APYX, Szymanski A, Bellamkonda RV. Agarose gel stiffness determines rate of DRG neurite extension in 3D cultures. Biomaterials. 2001; 22(10):1077–1084. [PubMed: 11352088]
43. Hopkins AMLL, Tortelli F, Spedden E, Staii C, Atherton TJ, Hubbell JA, Kaplan DL. Silk hydrogels as soft substrates for neural tissue engineering. Advanced Functional Materials. 2013; 23(41):5140–5149.

44. Spedden EWJ, Naumova EN, Kaplan DL, Staii C. Elasticity Maps of Living Neurons Measured by Combined Fluorescence and Atomic Force Microscopy. Biophysical Journal. 2012; 103(5):868–877. [PubMed: 23009836]
45. Loverde JROV, Aquino R, Lin L, Pfister BJ. Live imaging of axon stretch growth in embryonic and adult neurons. J of Neurotrauma. 2011; 28(11):2389–2403. [PubMed: 21663384]
46. Dadsetan MKA, Lu L, Windebank AJ, Yaszemski MJ. Stimulation of neurite outgrowth using positively charged hydrogels. Biomaterials. 2009; 30(23–24):3874–3881. [PubMed: 19427689]
47. Zhou ZYP, Geller HM, Ober CK. The role of hydrogels with tethered acetylcholine functionality on the adhesion and viability of hippocampal neurons and glial cells. Biomaterials. 2012; 33(8): 2473–2481. [PubMed: 22196899]
48. Lee DYCB, Park JH, Zhu SJ, Kim BY, Huh JY, Lee SH, Jung JH, Kim SH. Nerve regeneration with the use of a poly(L-lactide-co-glycolic acid)-coated collagen tube filled with collagen gel. J Craniomaxillofac Surg. 2006; 34(1):50–56. [PubMed: 16343912]
49. Rogers SLLP, Palm SL, McCarthy J, Furcht LT. Neurite extension by peripheral and central nervous system neurons in response to substratum-bound fibronectin and laminin. Dev Biology. 1983; 98(1):212–220.
50. Zuidema JMPM, Jaroch DB, Morrison FA, Gilbert RJ. Fabrication and charaterization of tunable poysaccharide hydrogel blends for neural repair. Acta Biomater. 2011; 7:1634–1643. [PubMed: 21130187]
51. Cheng C-MLP, Lin Y-W. Localized bimodal response of neurite extensions and structural proteins in dorsal-root ganglion neurons with controlled polydimethylsiloxane substrate stiffness. j Biomech. 2011; 44:856–862. [PubMed: 21208617]
52. Bunge RP. The role of the Schwann cell in trophic support and regeneration. J Neurol. 1994; 242:S19–S21. [PubMed: 7699403]
53. Koppes ANNA, Paolilo GM, Goodsell NM, Darwish HA, Zhang L, Thompson DM. Electrical stimulation of schwann cells promotes sustained increases in neurite outgrowth. Tissue Eng Part A. 2014; 20(3–4):494–506. [PubMed: 24063574]
54. KA N. Myelination and support of axonal integrity by glia. Nature. 2010; 468:244–252. [PubMed: 21068833]
55. Gu YJY, Zhao Y, Liu Y, Ding F, Gu X, Yang Y. The influence of substrate stiffness on the behavior and functions of Schwann cells in culture. Biomaterials. 2012; 33:6672–6681. [PubMed: 22738780]
56. Thompsen DMBH. Neurite outgrowth is directed by schwann cell alignment in the absence of other guidance cues. Ann Biomed Eng. 2006; 34(1):161–168. [PubMed: 16453203]
57. Hronik-Tupaj MRW, Tang-Schomer M, Omenetto FG, Kaplan DL. Neural responses to electrical stimulation on patterned silk films. J Biomed Mater Res A. 2013; 101(9):2559–2572. [PubMed: 23401351]
58. Yang JZC. Elevated potassium shortens action potential duration by altering outward currents in chick dorsal root ganglia neurons. J Neurobiol. 1990; 21(4):661–671. [PubMed: 2376736]
59. Shakhbazau AKJ, Hoyng SA, Kumar R, van Minnen J, Verhaagen J, Midha R. Early regenerative effects of NGF-transduced Schwann cells in peripheral nerve repair. Mol Cell Neurosci. 2012; 50(1):103–112. [PubMed: 22735691]

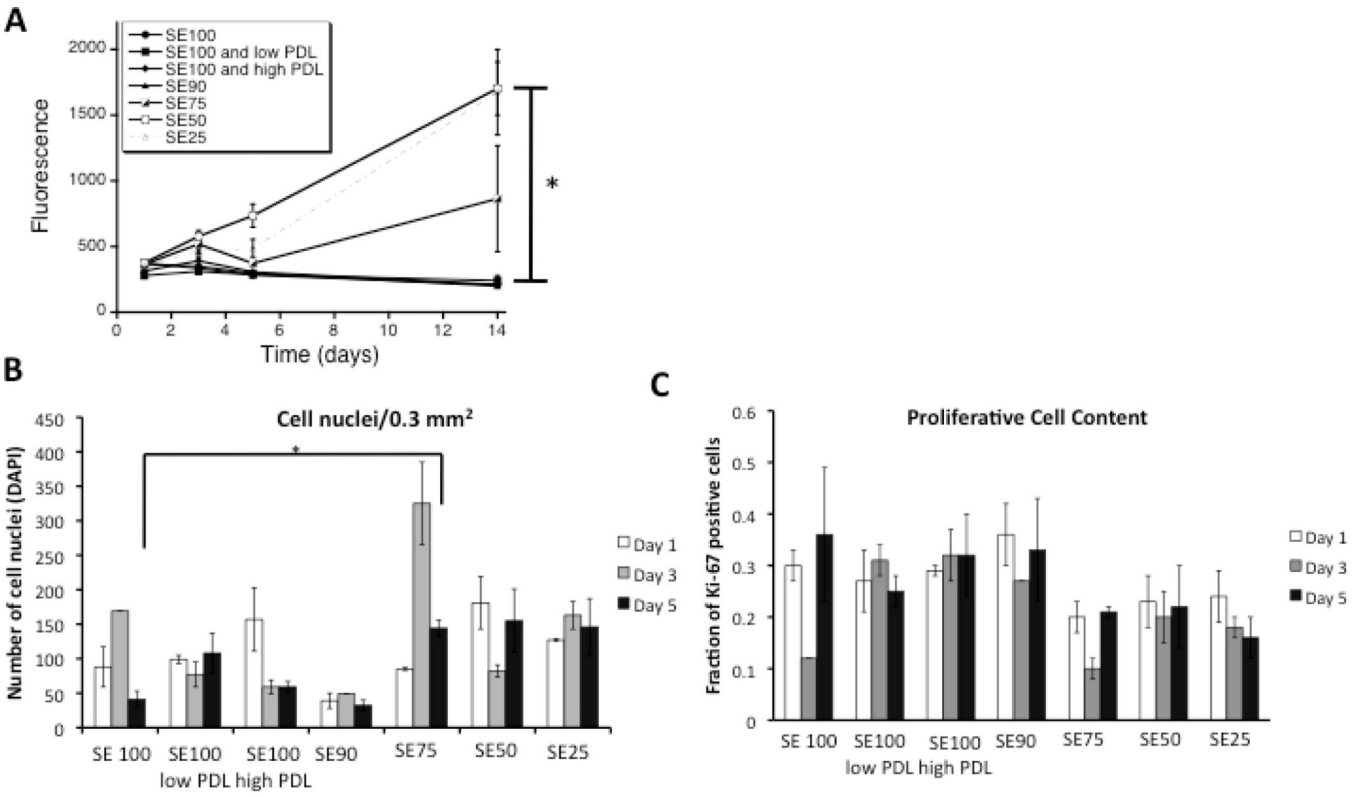

Figure 1.

A) Alamar blue metabolic activity for dissociated DRG neurons grown on silk alone, silk coated with 10 and 100 μg/mL PDL, and silk-tropoelastin films. Excitation wavelength 530 nm, Emission Wavelength 590 nm. Significant differences between (SE50, SE25) and (SE100, SE100 low PDL, SE100 high PDL, SE90) at day 14 were determined by ANOVA followed by Dunnett's post hoc test (*$P < 0.05$, n=3). B) Quantification of cell attachment using DAPI nuclear staining. The average number of cell nuclei for 3 areas of view (20×) are reported. Significant difference between cell attachment on day 5 was determined using a Student's T-test. C) Quantification of Ki-67 positive cells. Average values for three independent fields of view are presented with the standard error of the mean.

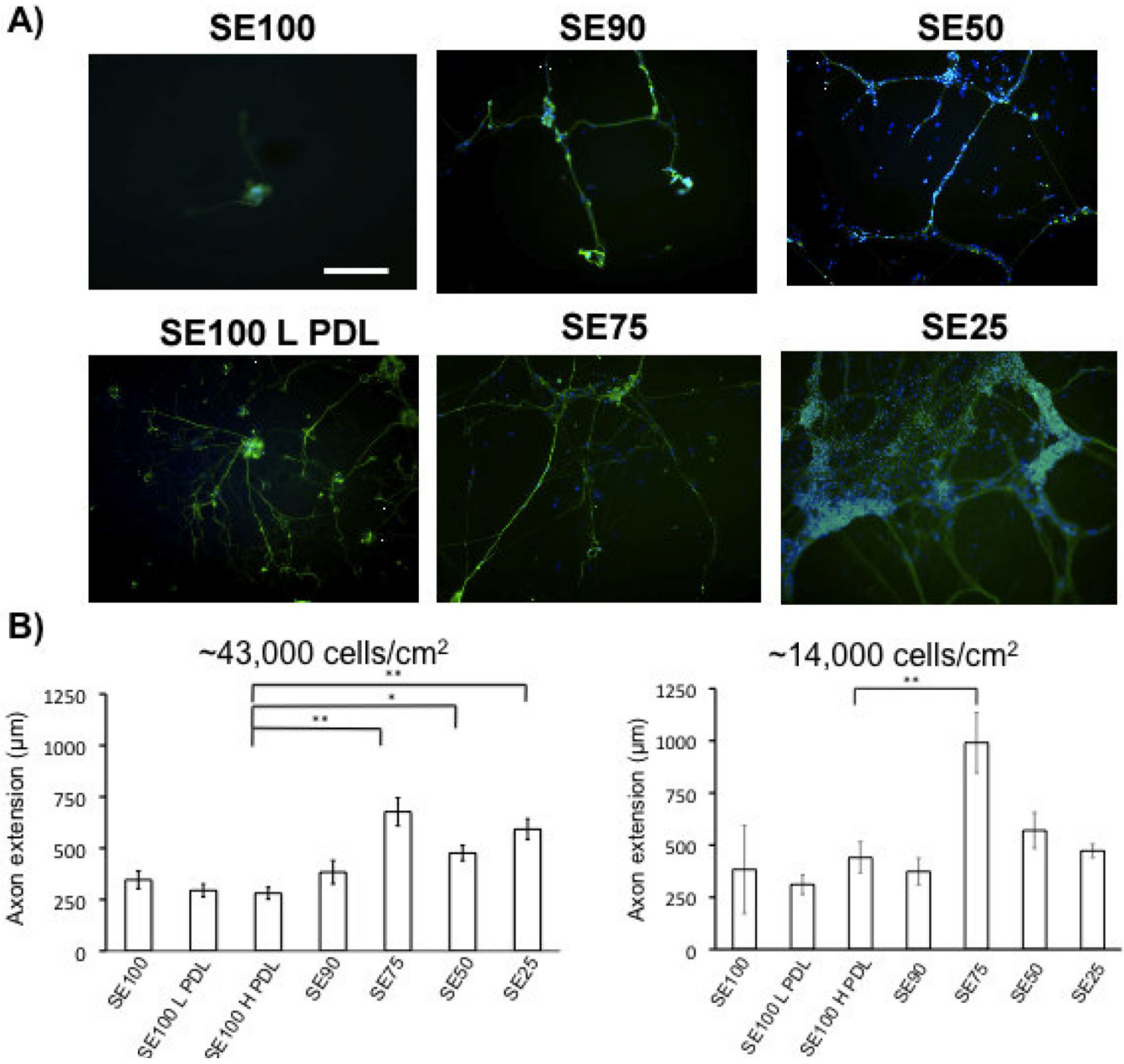

Figure 2.

A) βIII-tubulin (green) staining of DRG neurons grown on silk-tropoelastin films at day 4 (scale bar 250 μm). Nuclear staining with DAPI (blue). B) Quantification of axon extension (For high density, N=30 neurites were measured for each film condition, and taken from six independent fields of view. At low density, isolated neurons were measured, N = 5–10/ group). Protein films with tropoelastin contents higher than 25% (w/w) promoted longer axon growth than silk and PDL-coated silk conditions. Significant differences between silk-tropoelastin films and S100 were determined using ANOVA followed by Dunnett's post hoc test (P*<0.05, P**<0.01).

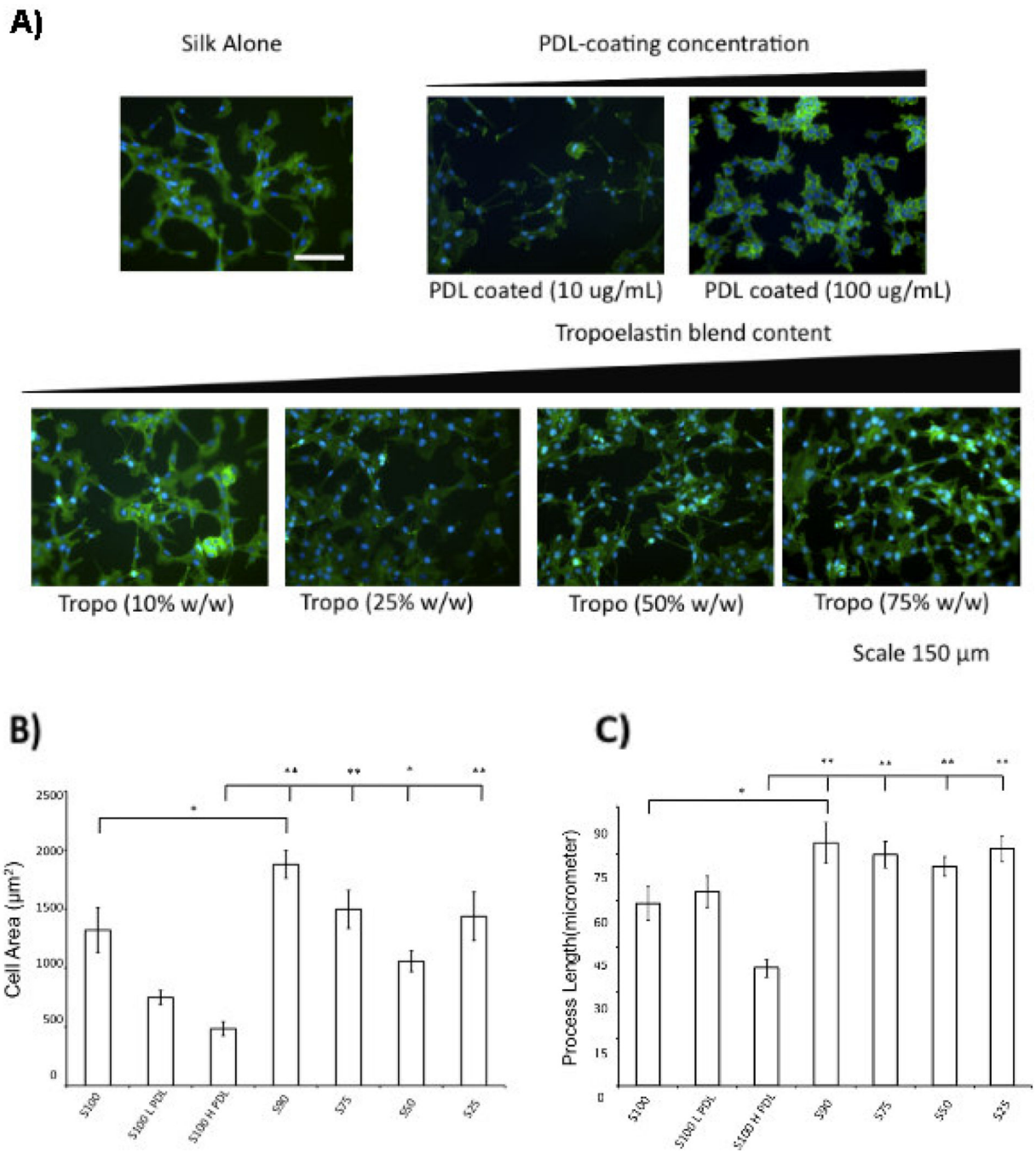

Figure 3.

A) Phalloidin staining (green) of Schwann cells grown on silk-tropoelastin films (day 4). B) Quantification of cell area and C) comparison of process length for each film composition. Significant differences between silk-tropoelastin conditions and S100-Low PDL were determined using ANOVA followed by Dunnett's post hoc test (P**<0.01, N=20–49). Scale bar is 150 µm.

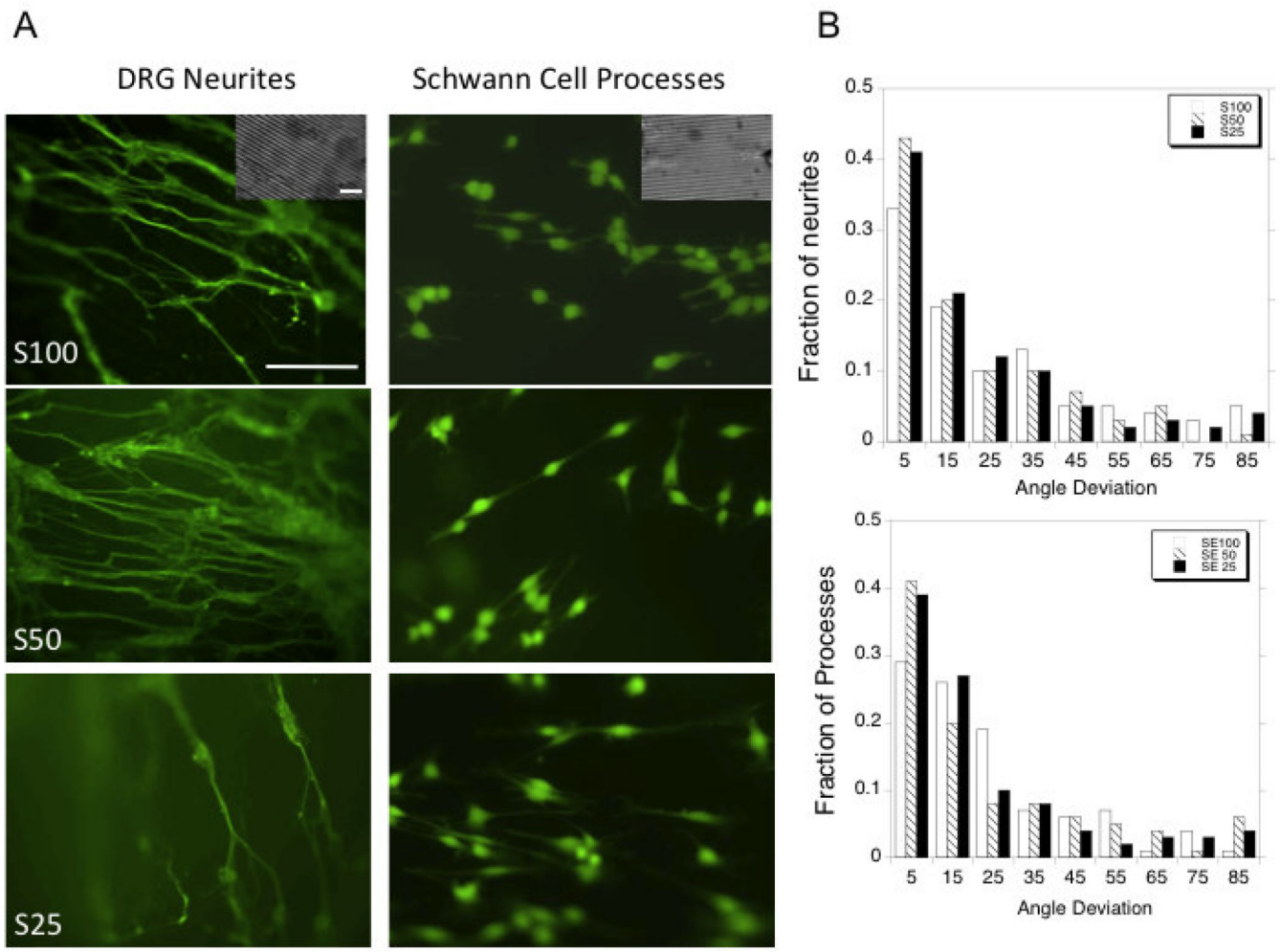

Figure 4.

A) Alignment of DRG neurites and Schwann cell processes on patterned films comprised of silk (100%), silk-tropoelastin (50/50), and silk-tropoelastin (25/75). DRG neurites were visualized with βIII-tubulin staining, Schwann cells were visualized using calcein AM staining. B) Quantification of neurite and Schwann cell process alignment. Scale bar is 150 μm. Scale bar for inset is 10 μm.

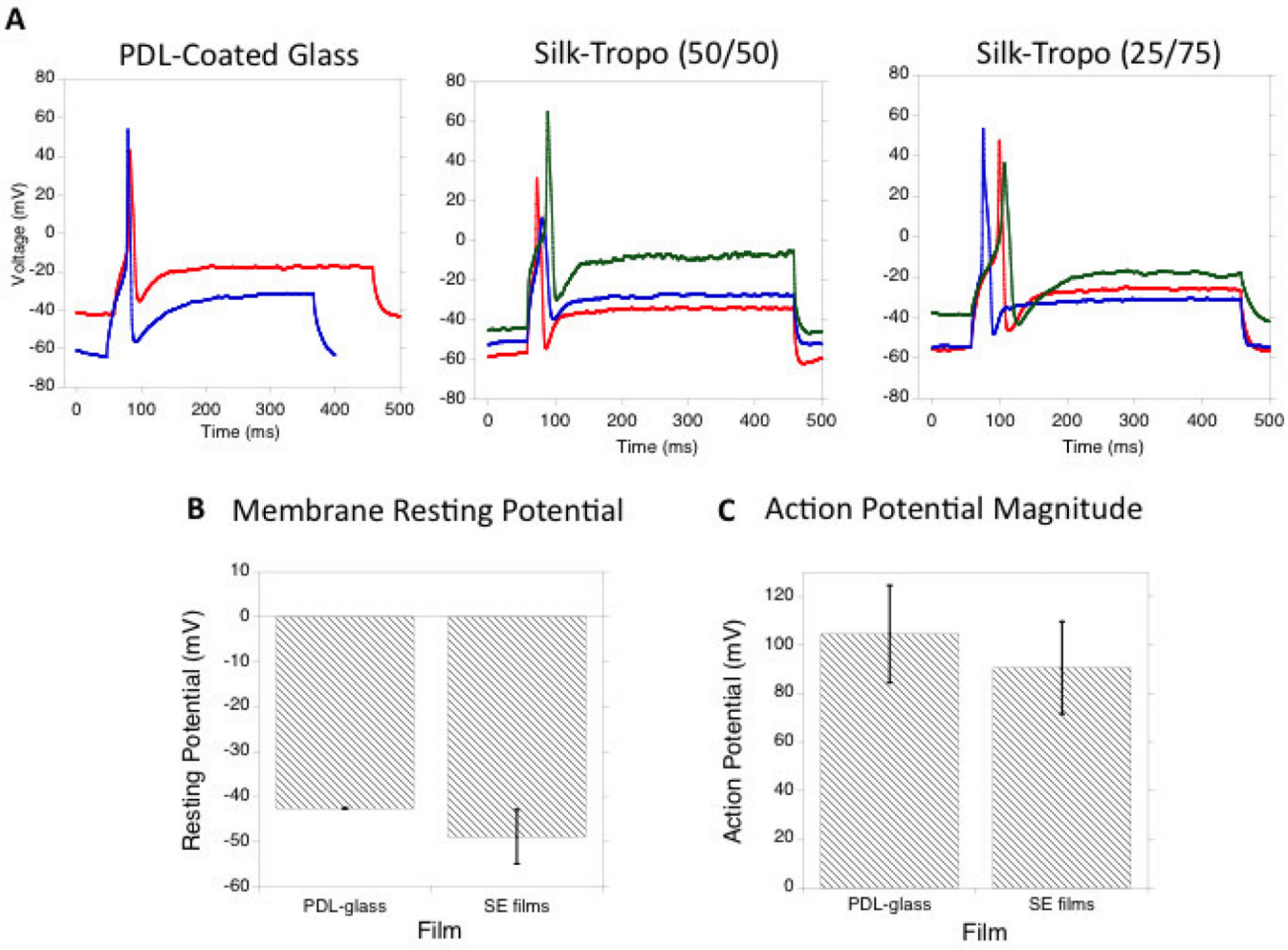

Figure 5.

A) Induced action potentials for neurons grown on PDL-coated glass, silk-tropoelastin (50/50), and silk-tropoelastin (25/75) surfaces. B) Comparison of membrane resting potential. C) Quantification of action potential magnitude for each surface. Significant differences between (SE50, SE25) and PDL-coated glass condition were calculated using ANOVA, ns=not significant, N=2 for PDL-glass and 3 for SE50, SE25.

Table 1

Mass ratios of blended silk-tropoelastin films, median and longest neurite measurement per image and average neuron cluster density. Neurite length and neuron density measurements are reported as the average value obtained from analysis of 6 independent films. Errors are reported as the standard error of the mean.

Sample	Mass Ratio [Silk/Tropoelastin]	Median Neurite Measured per Image (μm)	Longest Neurite Measured per Image (μm)	Neuron Cluster density (per mm^2)
S100	100/0	310 ± 55	556 ± 142	0.9 ± 0.4
S100 with L PDL[1]	100/0	302 ± 59	344 ± 54	1.4 ± 0.9
S100 with H PDL[1]	100/0	248 ± 55	467 ± 64	2.1 ± 1.1
S90	90/10	321 ± 67	598 ± 145	0.8 ± 0.2
S75	75/25	594 ± 97*	1140 ± 211**	2.2 ± 0.4
S50	50/50	449 ± 61	670 ± 83	4.3 ± 0.8*
S25	25/75	561 ± 41*	920 ± 184*	4.4 ± 0.6*

Significant differences to the S100 L PDL control were determined with one way ANOVA using Dunnett's post hoc test (P*<0.05, P**<0.01)

[1]. L PDL and H PDL indicate silk protein samples coated with 10 μg/mL and 100 μg/mL poly-D-lysine respectively.